ACS Catalysis

Research Article

pubs.acs.org/acscatalysis

Insight into the Effect of Water on the Methanol-to-Olefins Conversion in H-SAPO-34 from Molecular Simulations and in Situ Microspectroscopy

Kristof De Wispelaere,[†,‡] Caterina S. Wondergem,[§] Bernd Ensing,[‡] Karen Hemelsoet,[†] Evert Jan Meijer,[*,‡] Bert M. Weckhuysen,[*,§] Veronique Van Speybroeck,[*,†] and Javier Ruiz-Martínez[*,§]

[†]Center for Molecular Modeling (CMM), Ghent University, Technologiepark 903, 9052, Zwijnaarde, Belgium

[‡]Amsterdam Center for Multiscale Modeling and van 't Hoff Institute for Molecular Sciences, University of Amsterdam, Science Park 904, 1098 XH Amsterdam, The Netherlands

[§]Inorganic Chemistry and Catalysis, Debye Institute for Nanomaterials Science, Utrecht University, Universiteitsweg 99, 3584 CG Utrecht, The Netherlands

Supporting Information

ABSTRACT: The role of water in the methanol-to-olefins (MTO) process over H-SAPO-34 has been elucidated by a combined theoretical and experimental approach, encompassing advanced molecular dynamics simulations and in situ microspectroscopy. First-principles calculations at the molecular level point out that water competes with methanol and propene for direct access to the Brønsted acid sites. This results in less efficient activation of these molecules, which are crucial for the formation of the hydrocarbon pool. Furthermore, lower intrinsic methanol reactivity toward methoxide formation has been observed. These observations are in line with a longer induction period observed from in situ UV−vis microspectroscopy experiments. These experiments revealed a slower and more homogeneous discoloration of H-SAPO-34, while in situ confocal fluorescence microscopy confirmed the more homogeneous distribution and larger amount of MTO intermediates when cofeeding water. As such, it is shown that water induces a more efficient use of the H-SAPO-34 catalyst crystals at the microscopic level. The combined experimental−theoretical approach gives a profound insight into the role of water in the catalytic process at the molecular and single-particle level.

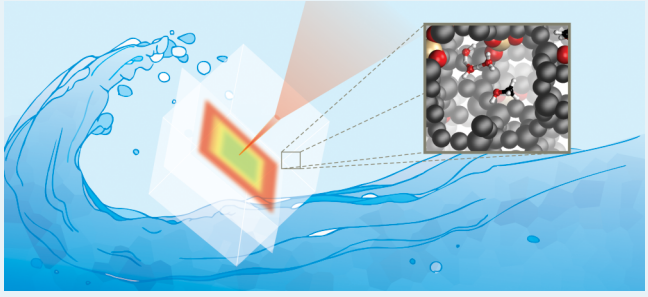

KEYWORDS: *methanol-to-olefins, zeolites, water, molecular dynamics, metadynamics, UV−vis spectroscopy, confocal fluorescence microscopy*

1. INTRODUCTION

The role of water in zeolite-catalyzed reactions is to date not fully understood, although water is often inherently part of process feeds and a byproduct of the catalytic process. Understanding the effect of water is currently very topical due to the development of zeolite-based biomass conversion processes, which contain and/or produce large amounts of water.[1,2] Specifically, during alcohol conversion into hydrocarbons, stoichiometric amounts of water are formed in the preequilibrium phase.[3] The conversion of methanol to hydrocarbons (MTH) over acidic zeolite or zeotype materials to produce gasoline (MTG), propene (MTP), or light olefins (MTO) is one of the most prominent technologies to bypass crude oil and has been industrialized in the past decade.[4−8]

Only a handful of papers describe the influence of cofeeding water on MTO conversion. Seminal work has been undertaken by Marchi and Froment and Wu and Anthony on the archetypal H-SAPO-34 catalyst, studying the impact of water on the MTO product distribution, coking, and efficiency of methanol conversion.[9,10] Furthermore, Marchi and Froment performed a similar study on mordenite-like zeolites.[11] More recently a study appeared by the group of Kapteijn on zeolite H-ZSM-58 bearing the DDR topology. This material proved to be an attractive catalyst for achieving high selectivity toward ethene and propene, comparable to that of H-SAPO-34, albeit with higher thermostability.[12] The DDR topology of H-ZSM-58 shows quite some similarity with the H-SAPO-34 material, as it also exhibits the typical cage structure separated by narrow 8-rings. For this type of material very interesting observations were found related to the influence of water on the MTO chemistry: cofeeding water increased the olefin selectivity, reduced the coking rate, and prolonged the catalyst life-

Received: September 24, 2015
Revised: December 21, 2015
Published: February 9, 2016

DOI: 10.1021/acscatal.5b02139
ACS Catal. 2016, 6, 1991−2002

time.[9,10,13] These effects were suggested to be caused by water occupying a fraction of the acid sites, making them unavailable for interaction with methanol or alkenes. These studies clearly show that obtaining a thorough understanding of the effect of water on the overall catalytic process is a complex task, as cofeeding water may affect various phenomena occurring at different time and length scales during the zeolite-catalyzed process, such as adsorption, diffusion, and intrinsic reactivity. As a consequence, the catalytic performance of the material will be modified. In this paper we aim at obtaining a deeper insight into the impact of water on the MTO process in H-SAPO-34 at the molecular and single-particle levels by using a unique complementary approach comprising advanced molecular simulations and in situ microspectroscopy experiments. Our approach reveals new observations on the effect of water during various MTO stages and the consequences of such an effect on the spatial distribution of aromatic species at the level of individual H-SAPO-34 particles.

To set the scene, one must acknowledge the overall complexity of the MTO chemistry, which has proven to be very difficult to unravel, due to many reactions occurring simultaneously.[4−6,14−16] In general, current insight allows distinguishing four successive reaction stages of the conversion in H-SAPO-34, as represented in Scheme 1,[6,17,18] and each of

Scheme 1. Schematic of the Stages during Methanol Conversion over a Solid Acid Zeolite Based Catalyst[a]

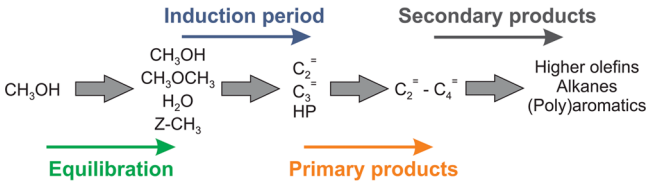

[a]Adapted with permission from ref 38. Copyright 2005 Springer.

them may be affected by the presence of water. In the equilibration phase, the addition of water shifts the equilibrium to the methanol side, as water is a reaction product of typical first-stage reactions. Water indeed reduces the formation of dimethyl ether (DME),[10] and an equilibrium shift was also observed by Hunger and co-workers when feeding water to a methylated H-SAPO-34 catalyst covered with methoxides.[19] During the induction period, a hydrocarbon pool (HP) is formed, taking the role as cocatalyst for product formation.[6,20−24] So far there is no full consensus concerning the mechanism governing the formation of such HP species.[25−27] One possibility concerns condensation reactions between initially formed ethene and/or propene, which might undergo oligomerization and cyclization reactions.[25,27] Previous experimental studies on the effect of feed composition on the MTO process suggested that water might alter the adsorption/desorption behavior of these primary products and as such affect their reactivity.[10] Furthermore, as methoxides are believed to play a crucial role during the induction period,[19,27−29] it is probable that the aforementioned water-induced equilibrium shift also affects the second stage of the MTO reaction. There are indications that water can play an important role in the formation of the primary products: e.g., by assisting the protonation and deprotonation of the active aromatic species during the formation of olefins.[30,31] Finally, secondary reaction products including less active polyaromatic compounds are formed, as can be seen in UV−vis spectra of catalyst samples under MTO conditions.[32−35] This coke formation eventually leads to catalyst deactivation by pore[36] and/or site[37] blocking. It has been reported that the deactivation rate was substantially decreased by water addition to the feed.[10]

Researchers have attempted to increase the stability of H-SAPO-34, the archetypal MTO catalyst,[39,40] by decreasing the particle size,[41−43] creating a secondary network of meso- and macropores[44] and addition of water in the feed.[9−11,23,45,46] For H-SAPO-34 catalysts at 400 °C it was reported that an optimal feed consists of 73−80 mol % of water to minimize the coking rate and maximize the olefin selectivity. Under these conditions, the H-SAPO-34 crystals were able to process eight times more methanol than with a pure feed prior to deactivation.[9,10,23,45,46] Similar results were reported by Kapteijn and co-workers for the DDR-structured H-ZSM-58 catalyst.[12] These studies are of high relevance, considering that the methanol feed often contains considerable amounts of water[47−49] as a byproduct of methanol production from syngas.[50−52] The beneficial effect of water and its presence in methanol production as an impurity shows that a profound understanding of the effect of water on the MTO reaction is urgently needed.

In this study we provide theoretical and experimental evidence for the delicate impact that water has on various stages of the catalytic process by combining intimately molecular simulations mimicking operating conditions as close as possible and in situ microspectroscopy experiments at the single-catalyst particle level.

2. EXPERIMENTAL AND THEORETICAL SECTION

2.1. Computational Details. Modeling zeolite-catalyzed reactions under conditions that approach true experimental or industrial conditions is a complex task.[18,53−62] The typical framework flexibility exhibited by zeolites, the influence of surrounding solvent molecules, and entropic and temperature effects cannot be fully captured by well-established static methods and require an approach in which larger portions of the potential energy surface (PES) can be explored. In this study, we mainly aim to assess the influence of multiple protic molecules on methanol adsorption, activation, and reactivity. Therefore, we opted to apply density functional theory (DFT) based molecular dynamics (MD) techniques to study zeolite-catalyzed reactions. MD simulations only recently entered the field of zeolite catalysis, and their potential is currently being explored and demonstrated.[18,53−62]

Our MD simulations were performed with the CP2K software package,[63] using a revPBE-D approach including Grimme D3 dispersion corrections,[64] a DZVP basis set, and GTH pseudopotentials. A first set of MD simulations on different methanol−water mixtures has been performed in the NPT ensemble at 330 °C and around ambient pressure, with a time step of 0.5 fs during 50 ps in a H-SAPO-34 unit cell containing two Brønsted acid sites (BAS). Such a unit cell represents a catalyst with a Si/(Al + P) ratio of 0.059. Since we mainly simulate local effects around the 8-ring containing the two acid sites, we opted to limit the number of BAS per unit cell to two (see section S1 of the Supporting Information). As illustrated in Scheme 2, we adopted a variety of methanol−water (mw) mixtures, denoted as $(x{:}y)_{\mathrm{mw,sim}}$ with x and y being the number of methanol and water molecules per BAS, respectively.

With a recently developed semianalytical mean-field model based on the osmotic ensemble, we checked to what extent the

DOI: 10.1021/acscatal.5b02139
ACS Catal. 2016, 6, 1991−2002

Scheme 2. Simulated Loadings of Methanol-Water Mixtures in H-SAPO-34 with Indication of the Acid Sites[a]

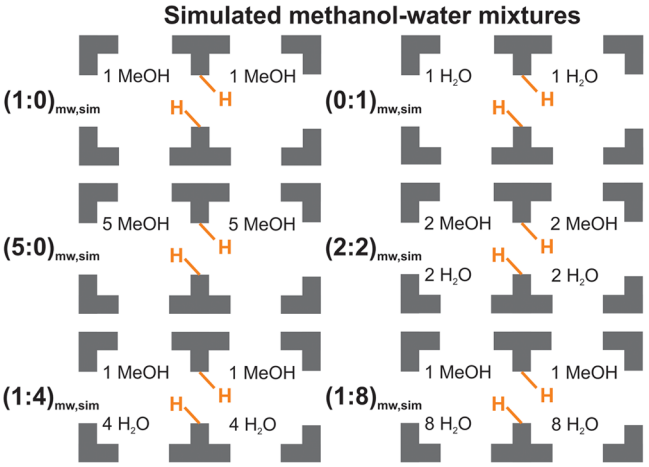

[a] $(x{:}y)_{mw,sim}$ stands for x MeOH and y H_2O molecules per BAS.

simulated conditions correspond to realistic process conditions. Starting from the interaction energy between a guest molecule and the nanoporous material and the accessible pore volume, the loading of the material can be estimated.[65] A rough estimate of the adsorption enthalpy of methanol not directly interacting with the zeolite's BAS—i.e. methanol does not form a hydrogen bond with the acid site—was obtained from MD simulations. We found values in the range of 40−60 kJ/mol, which correspond well with calculated adsorption enthalpies for methanol in silicalite in the range from 46 to 66 kJ/mol using periodic PBE-D and the nonlocal correlation functional vdW-DF2.[66] Furthermore, it was assumed that 65% of the total unit cell volume is accessible, as reported by First et al.[67] It was then calculated that H-SAPO-34 pores in contact with a pure methanol feed at pressures ranging from 0.1 to 5 bar are typically loaded with 10−13 methanol molecules. Note, however, that the simulated loadings denoted as $(x{:}y)_{mw,sim}$ in Scheme 2 are single-site conditions and do not necessarily correspond to methanol−water compositions of the feed during the experiments. To accurately calculate adsorption isotherms, one needs to rely on grand canonical Monte Carlo (GCMC) simulations. With such an approach Kuhn et al. found that water addition enhances the methanol loading of H-ZSM-58 in comparison to pure methanol adsorption.[68] However, a GCMC study is beyond the scope of this work.

Next, an additional set of MD simulations in the NVT ensemble at 330 °C has been performed on different propene−water (pw) mixtures denoted as $(x{:}y)_{pw,sim}$ with x and y being the number of propene and water molecules per BAS (Scheme 3). Hereby we used the time-averaged cell parameters of the $(1{:}8)_{mw,sim}$ simulation (Table S1 in the Supporting Information).

Adsorption enthalpies of methanol and water were determined according to

$$\Delta H_{ads,330^\circ C} = \langle U_{complex}\rangle - \langle U_{zeolite}\rangle - \langle U_{guest}\rangle - RT \quad (1)$$

in which $\langle U_{complex}\rangle$, $\langle U_{zeolite}\rangle$, and $\langle U_{guest}\rangle$ are the average total energies of H-SAPO-34 with one guest molecule adsorbed per BAS (the $(1{:}0)_{mw,sim}$ and $(0{:}1)_{mw,sim}$ loadings according to Scheme 2), the empty framework, and the guest molecule in the gas phase and R is the universal gas constant. Each of these

Scheme 3. Simulated Loadings of Propene−Water Mixtures in H-SAPO-34 with Indication of the Acid Sites[a]

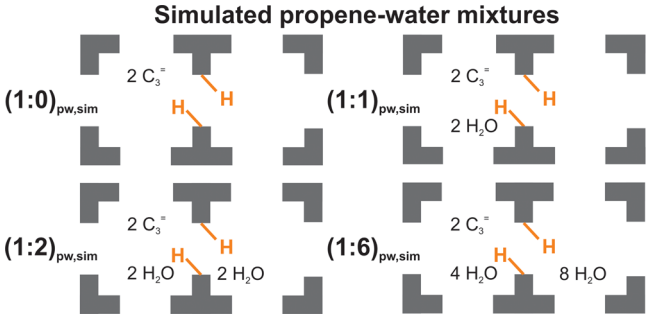

[a] $(x{:}y)_{pw,sim}$ stands for x $C_3^=$ and y H_2O molecules per BAS.

averages were obtained from separate 50 ps MD simulations, meaning that additional MD simulations of the empty framework in the NPT ensemble and the guest molecule in the gas phase in the NVT ensemble were conducted at 330 °C. A similar approach was recently adopted by Hafner and co-workers.[56,57] Statistical errors on adsorption enthalpies were obtained by block averaging the average total energies in eq 1.

The formation of methoxides, which is a rare event, was studied using metadynamics (MTD) simulations at 330 °C in the NVT ensemble, using the optimized cell parameters from the NPT runs. This advanced sampling technique is used to enhance the probability of sampling chemical reactions or rare events and requires the definition of a limited number of collective variables describing the reaction coordinate.[69−73] Methoxide formation in this study was sampled with two collective variables defined as coordination numbers (CN):

$$\mathrm{CN} = \sum_{i,j} \frac{1 - (r_{ij}/r_0)^{nn}}{1 - (r_{ij}/r_0)^{nd}} \quad (2)$$

as depicted in Scheme 4. The first CN describes the C−O bond cleavage of methanol, and the second CN describes the

Scheme 4. Schematic of the Two Coordination Numbers (CN) Applied during the Metadynamics Simulations of Methoxide Formation[a]

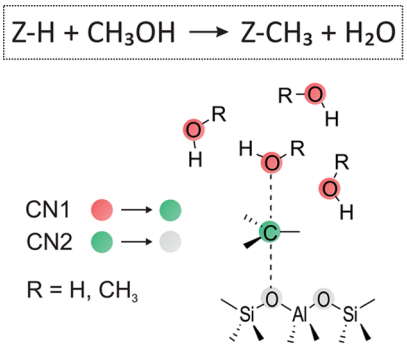

[a] The R−OH molecules represent surrounding protic molecules, which can be water or methanol.

formation of a covalent bond between the methyl carbon and the eight framework oxygen atoms surrounding the two BAS in the H-SAPO-34 unit cell. We used the MTD approach as implemented in the CP2K software package.[63]

DOI: 10.1021/acscatal.5b02139
ACS Catal. 2016, 6, 1991−2002

The lowest free energy paths (LFEP) were calculated as described in refs 53 and 73. Given the free energy profile, the corresponding free energy barrier $\Delta G^{\ddagger}$ was conveniently computed from the probability density at the top of the barrier compared to the reactant state probability:

$$\Delta G^{\ddagger} = -\frac{1}{\beta}\ln\frac{\exp[-\beta G(\mathrm{TS})]}{\int_{-\infty}^{\mathrm{TS}}\exp[-\beta G(s)]\,\mathrm{d}s} \quad (3)$$

where $\beta = 1/k_B T$ and TS is the position at the top of the barrier along the normalized reaction coordinate (s). Statistical errors on free energy barriers were computed as the standard deviation of the mean after removal of correlated data values. More details on the applied unit cell, optimized cell parameters, and more details on the settings for the metadynamics simulations can be found in section S1 of the Supporting Information.

2.2. Microspectroscopy Experiments. The MTO experiments were targeted for understanding the effect of water on the length of the induction period and the distribution and evolution of hydrocarbon pool species over H-SAPO-34 in a time- and space-resolved manner. For this purpose, we used optical spatiotemporal spectroscopic techniques and micron-sized H-SAPO-34 crystals. The as-synthesized H-SAPO-34 crystals are cubic in shape and have a size of 50 × 50 × 50 μm^3, and their synthesis procedure is reported elsewhere.[74] The Si/(Al + P) ratio is 0.204, which corresponds theoretically with two BAS per chabazite cage. These micron-sized H-SAPO-34 crystals are model systems and possess a uniform spatial distribution of Brønsted acid sites.[33] Additionally, these crystals have an optimum size for their study with our micro-spectroscopic tools. The in situ catalytic reactions were performed in a custom-made in situ cell that had a low dead volume and was made of stainless steel with a 0.2 mm quartz lid on the top. The in situ cell was heated by the heating element of a THMS600 Linkam cell. For all of the in situ experiments a total flow of 50 mL/min was used. Water and methanol were introduced by flowing N_2 through saturators with the reagents, which were kept at 20 °C. The N_2 flow through the methanol saturator was always set at 0.75 mL/min in order to keep a constant methanol concentration in the gas stream. Water contents were varied by adjusting the N_2 flow through the water saturator. The formation of active and deactive aromatic species in individual H-SAPO-34 crystals was monitored by UV−vis microspectroscopy. The UV−vis microspectroscopy measurements were performed with an Olympus BX41 upright microscope connected to an Avantes AvaSpec-2048TEC UV−vis spectrometer by using a 50 × 0.5 NA high-working-distance microscope objective lens. The samples were illuminated with a 75 W tungsten lamp. The microscope setup was equipped with a 50/50 double-viewport tube, which accommodated a charge-coupled device (CCD) video camera (ColorView IIIu, Soft Imaging System GmbH) and an optical fiber mount. The microscope was connected to a CCD UV−vis spectrometer (AvaSpec-2048TEC, Avantes) by a 200 mm core fiber. Spectra were recorded in absorbance mode and saved automatically every 5 s from the moment that methanol was introduced into the system. The integration time and average for each spectrum were 50 and 100 ms, respectively. The detection range was 390−751 nm. Spectra were recorded in the middle of a crystal with a spot size of 2 μm. The H-SAPO-34 crystals were used as a white reference, and a black reference was obtained by shuttering the UV−vis spectrometer. Confocal fluorescence microscopy was applied to gain complementary information on the spatial distribution of the distinct aromatic species. This was done with the same in situ cell and reaction conditions in order to directly compare both results. These confocal fluorescence microscopy experiments were performed using a Nikon Eclipse 90i upright microscope with a 50 × 0.55 NAdry objective lens. Confocal fluorescence microscopy images were collected by a Nikon A1-SHR A1 R scan head connected to two Mellers Griot laser light sources with emission wavelength of 488 nm (ion laser, 150 mW) and 561 nm (yellow diode-pumped solid-state laser, <50 nW). The detection ranges used were 500−550 and 570−620 nm, respectively. The fluorescence images were taken 18 μm inside the crystal. More details about the cell design and experimental details can be found in section S2 of the Supporting Information.

3. RESULTS AND DISCUSSION

3.1. Activation of Reactants at the Molecular Level. With advanced molecular simulations we aim at studying the specific role of water at the molecular level. Inspired by earlier reported hypotheses, we more specifically study the competition at the BAS between water and methanol or propene. Methanol activation by the BAS is of importance during all stages of the MTO reaction. During the induction period (Scheme 1), propene activation for dimerization and cyclization is a crucial step for the formation of cyclic HP species.

3.1.1. Competition between Water and Methanol. A first insight into the role of water at the molecular level is obtained from DFT-based MD simulations, which demonstrate that water and methanol compete to have direct access to the BAS in the initial stage of the reaction, as outlined hereafter. From simulations of pure methanol or water adsorbed in H-SAPO-34, i.e. the $(1{:}0)_{mw,sim}$ and $(0{:}1)_{mw,sim}$ compositions in Scheme 2, we calculated methanol and water adsorption enthalpies at 330 °C of −90 and −75 kJ/mol, respectively (Table 1).

Table 1. Calculated and Measured Adsorption Enthalpies of Methanol and Water in H-SAPO-34 (This Work) and H-ZSM-5 (References 75−77)

	dynamic[a] H-SAPO-34 330 °C	static[70,74] H-ZSM-5 130 °C	exptl[70−72] H-ZSM-5 130 °C
ΔH_{ads} (kJ/mol)			
methanol	−90	−112	−115
water	−75	−91	−90

[a]Estimated error bars of 10 kJ/mol on the calculated values.

These calculated values are lower than reported values for H-ZSM-5, as summarized in Table 1.[75−77] The lower values may be attributed to the intrinsic lower acid strength of H-SAPO-34[78] and thermal effects at 330 °C. Indeed, at higher temperatures methanol and water may adopt conformations where the adsorbates are not directly interacting with the BAS, resulting in relatively lower average adsorption enthalpies (see section S3 of the Supporting Information). From the MD results, it was estimated that methanol and water are not interacting with the BAS during 24% and 14% of the 50 ps simulations. Similar effects were observed recently by Göltl et al. for alkane adsorption.[57] In earlier work adsorption energies for methanol adsorption in H-SAPO-34 using static theoretical methods have been reported, which are on the same order of magnitude as our dynamically obtained results.[79] To the best of

DOI: 10.1021/acscatal.5b02139
ACS Catal. 2016, 6, 1991−2002

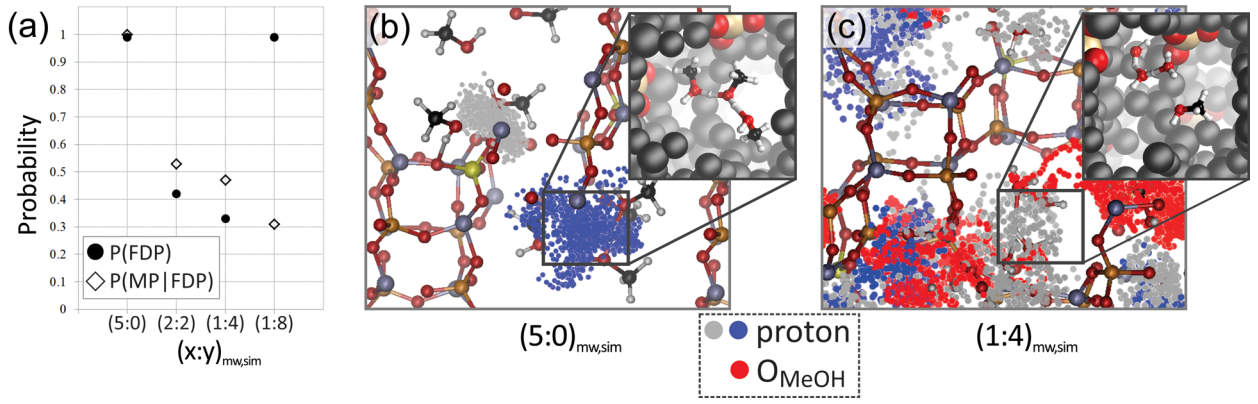

Figure 1. (a) Probability for framework deprotonation (FDP) and probability of methanol protonation when the framework is deprotonated (MP|FDP) during 50 ps MD simulations of different methanol−water mixtures adsorbed in H-SAPO-34 at 330 °C and around ambient pressure. (b, c) H-SAPO-34 loaded with a $(5:0)_{mw,sim}$ and $(1:4)_{mw,sim}$ methanol−water mixture. The gray, blue, and red dots represent the positions of the two acid protons and methanol oxygen atoms, respectively. The insets show snapshots of the MD run with highlighted acid sites. $(x:y)_{mw,sim}$ stands for a simulation with x MeOH and y H_2O molecules per BAS.

our knowledge, no experimentally measured adsorption enthalpies for methanol in H-SAPO-34 have been reported. Our single-molecule adsorption results show that both protic molecules have a strong adsorption capability in H-SAPO-34.

The competition between water and methanol to form a hydrogen bond with the BAS in H-SAPO-34 was explicitly studied during an MD simulation of H-SAPO-34 loaded with one water and one methanol molecule per acid site ($(1:1)_{mw,sim}$ in Figure S7 in the Supporting Information) at 330 °C. A nearly equal probability of water and methanol occupying a single BAS was observed (Figure S8 in the Supporting Information), indicating that water and methanol are indeed able to compete for the BAS. This observation was not found to depend on the acid site density (see section S1 of the Supporting Information). This competition of water with oxygenates and hydrocarbons for acid sites was already suggested in the early 1990s by Marchi and Froment after their experiments on the MTO reaction in H-SAPO-34 with a water-containing feed.[9]

A second insight was obtained from MD simulations performed on the catalyst loaded with multiple methanol and water molecules ($(5:0)_{mw,sim}$, $(2:2)_{mw,sim}$, $(1:4)_{mw,sim}$, and $(1:8)_{mw,sim}$; see Scheme 2), which demonstrate that methanol protonation becomes less probable due to the competitive adsorption of both molecules at the BAS. Methanol protonation is the elementary activation step before any reaction in which it participates may occur. From the systematic set of MD simulations at 330 °C and around ambient pressure we calculated the probabilities for framework deprotonation (FDP) and methanol protonation once the framework is deprotonated (MP|FDP), as shown in Figure 1a. For a pure methanol loading $(5:0)_{mw,sim}$, a 100% probability for framework deprotonation was observed, in agreement with earlier findings.[53] It was earlier shown that these clusters are able to modify the intrinsic methanol reactivity in comparison to a genuine reaction at the BAS.[61,62] A distinct effect of water addition is observed when a methanol−water mixture is considered ($(2:2)_{mw,sim}$, $(1:4)_{mw,sim}$, $(1:8)_{mw,sim}$), as illustrated in Figure 1a. A lower apparent proton affinity of mixed methanol−water clusters in comparison to pure systems induces a lower degree of framework deprotonation when water is added. For intermediate to high loadings of water ($(2:2)_{mw,sim}$ and $(1:4)_{mw,sim}$) the probability for framework deprotonation drops to 42 and 32%, respectively. Very high water loadings $(1:8)_{mw,sim}$ are required to obtain a similar probability for framework deprotonation as obtained with pure methanol. In earlier work by some of the present authors it has been reported that the H-SAPO-34 framework gets deprotonated with a probability of 100% by five methanol or eight water molecules per BAS.[53] That such high water loadings are needed to fully deprotonate the framework explains the sharp increase in P(FDP) in Figure 1a. These findings are also in line with other theoretical studies based on static and dynamic approaches, stating that two methanol molecules are already able to deprotonate a zeolitic BAS,[80−84] whereas for water the formation of larger clusters is required.[85−88] Also note that the absolute values of the calculated probabilities depend on the acid site density of the H-SAPO-34 material (see section S1 of the Supporting Information).

To connect the observation of framework deprotonation with methanol reactivity, the probability of methanol protonation once the framework is deprotonated was probed, and the results are also depicted in Figure 1a. This probability can be interpreted as the availability of the protons to methanol or its tendency to participate in reactive events. As expected, this availability decreases from 100% for pure methanol to 53%, 47%, and 31% for methanol−water mixtures with $(2:2)_{mw,sim}$, $(1:4)_{mw,sim}$, and $(1:8)_{mw,sim}$ compositions, respectively. This suggests that when protonated clusters are formed it becomes less likely that methanol gets protonated. Figure 1b displays the distribution of the protons (blue and gray dots) during the MD simulation of H-SAPO-34 loaded with pure methanol ($(5:0)_{mw,sim}$), whereas Figure 1c displays the analogue for a $(1:4)_{mw,sim}$ methanol−water mixture. Next to the positions of the protons, the trajectories of the methanol oxygen atoms (red dots) are displayed. As the red dots and the gray and blue dots only partially overlap for the $(1:4)_{mw,sim}$ conditions, this indicates that, during a significant time in the simulation, methanol has no access to a proton, preventing it from getting activated for further reaction.

The effect of water on the nature of the BAS could also be demonstrated by a vibrational analysis via calculated velocity power spectra (VPS), showing a broadening of the OH stretching region, indicative of interactions between the hydrophilic framework and formation of hydrogen-bonded water clusters (Figure S9 in the Supporting Information).

DOI: 10.1021/acscatal.5b02139
ACS Catal. 2016, 6, 1991−2002

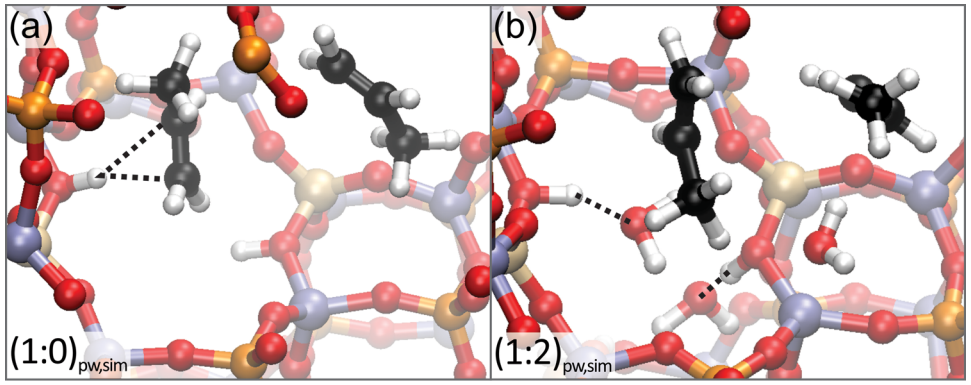

Figure 2. Snapshots of two propene molecules adsorbed in a CHA cage of H-SAPO-34 from an MD simulation at 350 °C (a) in the absence of water $(1:0)_{pw,sim}$ and (b) in the presence of water $(1:2)_{pw,sim}$, with $(x:y)_{pw,sim}$ standing for x propene molecules and y water molecules per BAS.

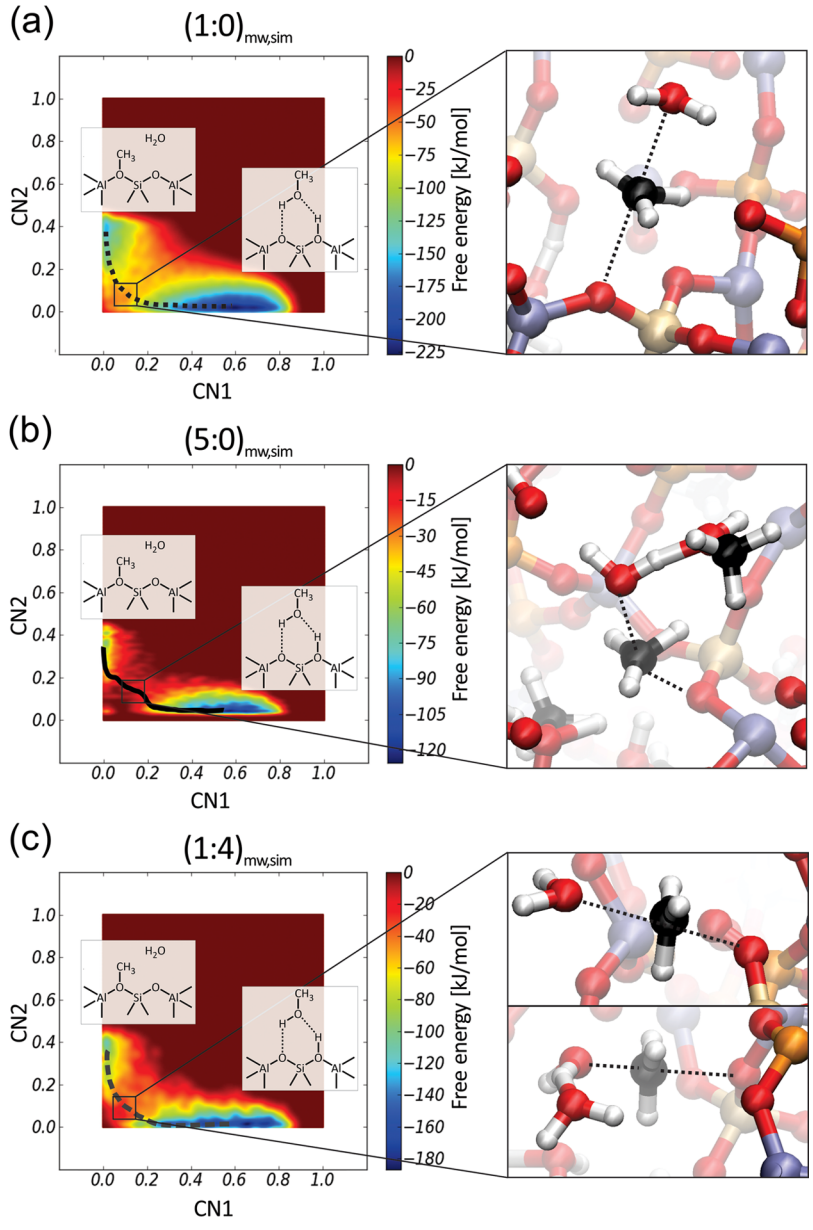

Figure 3. 2D FES at 330 °C for methoxide formation in pure methanol $(1:0)_{mw,sim}$ and $(5:0)_{mw,sim}$ (a, b) and the $(1:4)_{mw,sim}$ methanol–water mixture (c) occluded in H-SAPO-34, with indication of the LFEP. The insets show snapshots of the TS region. $(x:y)_{mw,sim}$ stands for x MeOH and y H_2O molecules per BAS.

DOI: 10.1021/acscatal.5b02139
ACS Catal. 2016, 6, 1991–2002

These simulations thus point out that methanol and water compete for direct access to the BAS, resulting in a less efficient methanol protonation.

3.1.2. Competition between Water and Propene. In the previous section we focused on the competition between methanol and water at the BAS, as methanol is the primary reactant for many crucial steps during the MTO process. The primary MTO products ethene and propene are known to be important reactants during the induction period (Scheme 1) for the formation of the HP, mainly consisting of polymethylated benzenes in H-SAPO-34.[24,32,34] Interestingly, Wu and Anthony suggested that the reduced coking rate upon water addition to the methanol feed in H-SAPO-34 can be attributed to the competition between olefins and water, which could hamper olefin conversion to cyclic HP species and cokes, keeping the channels inside the catalyst unblocked.[10] In this view we have performed an additional set of MD simulations to explicitly sample the competition between propene and water for direct access to the BAS in H-SAPO-34.

It is highly debated how the first C−C bond is formed during the MTO process, but once primary products such as ethene and propene are formed, they can oligomerize to form precursors for aromatic HP species. This was also investigated by Vandichel et al. with a DFT study. They proposed a mechanism starting from the formation of a framework-bound propoxide from propene, followed by dimerization with another propene molecule to form the 2-hexyl carbenium ion. A subsequent ring closure might then lead to the formation of active HP compounds.[25] In view of this, it is important to investigate the influence of water on the direct interaction of propene with the BAS. Moreover, the formation of HP species was recently found to be rate determining during the induction period in H-ZSM-5.[89]

In the absence of water, i.e. for the propene−water mixture $(1{:}0)_{pw,sim}$ in Scheme 3, one of the propene molecules adsorbed in a CHA cage of H-SAPO-34 forms a π complex with the BAS, as shown in Figure 2a. When water is present around the BAS, we indeed observe that water and propene compete for access to the BAS. Water is able to quickly replace propene and occupy the BAS, as shown in Figure 2b for the $(1{:}2)_{pw,sim}$ propene−water mixture (Scheme 3). With an increasing amount of water, this behavior becomes even more pronounced. This observation suggests that water lowers the coverage of propene at the BAS, decreasing the probability that propene gets activated for further reaction toward the formation of cyclic HP species. As a result, this would imply that the active cycle based on aromatic HP species gets delayed by a longer induction period.

In general, water thus lowers the amount of BAS occupied by reactant molecules such as methanol and propene. It can thus be anticipated that the reduced activation of these molecules will alter the kinetics of some MTO reaction stages.

3.2. Methanol Reactivity during the Early Stages of the MTO Conversion. After the assessment of the effect of water on methanol and propene adsorption and activation, the intrinsic reactivity of methanol has been investigated by studying the formation of framework-bound methoxide species. These are predominant species during the induction time (see Scheme 1) and can further act as methylating agents during the MTO reaction.[19,26,27,29,90] In this view the work of Hunger et al. is worth mentioning, as they pretreated zeolite catalysts to cover the acid sites with methoxides to demonstrate the role and high reactivity of surface methoxides during the induction period and product formation of the MTO process.[19,91,92] From a thermodynamic point of view, water can affect the formation of methoxide species by shifting the equilibrium toward the formation of methanol.[19] In addition to these thermodynamic implications, our simulations suggest that the presence of water decreases methanol's intrinsic reactivity toward methoxide formation. To this end, metadynamics simulations at 330 °C were carried out for the $(1{:}0)_{mw,sim}$, $(5{:}0)_{mw,sim}$, and $(1{:}4)_{mw,sim}$ methanol−water mixtures (Scheme 2), corresponding to a low and high loading of pure methanol and a mixture with an excess of water. As such, the influence of an identical number of surrounding methanol or water molecules could be assessed. Hereby, the $(1{:}0)_{mw,sim}$ simulation was used as a reference, as a loading of one methanol molecule per BAS does not allow the assistance of other protic molecules during the reaction.

Figure 3 displays the calculated 2D free energy surfaces (FES), lowest free energy paths, and some selected snapshots of the transition region for methoxide formation in the different methanol−water mixtures. The shapes of the FESs and LFEPs are quite similar for the three cases considered; however, a detailed analysis of the sampled trajectories and free energy profiles reveals distinct differences among the three considered simulations and gives insight into the effect of water on the kinetics of methoxide formation. For this purpose, the two-dimensional FES was projected onto a one-dimensional reaction coordinate, which was obtained by calculating the LFEP according to the procedure proposed by Ensing et al.[73]

The one-dimensional free energy profiles in Figure 4 show that the free energy barrier for methoxide formation in the absence of additional guest molecules (167 ± 4 kJ/mol) is higher than in the case where additional water (147 ± 5 kJ/mol) or methanol (123 ± 2 kJ/mol) molecules are present to assist the reaction. Fan and co-workers earlier reported a free energy barrier of 141 kJ/mol at 400 °C for the H-SAPO-34 catalyzed methoxide formation assisted by one additional methanol molecule, on the basis of static periodic PBE calculations.[26] Note that our value (123 ± 2 kJ/mol) differs as we take into account the presence of more methanol molecules and due to the dynamic approach required to fully capture the complexity of the assisting effect of multiple protic molecules.[62] The results show that the facilitating effect of

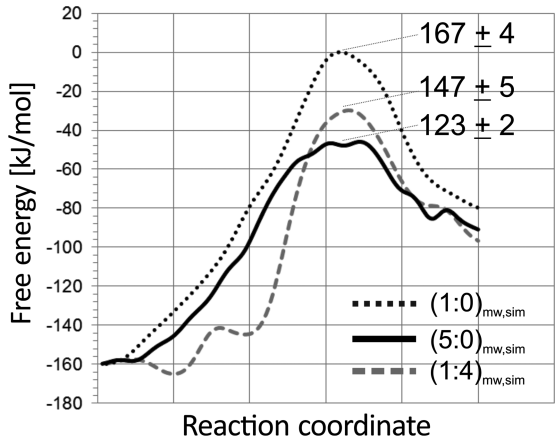

Figure 4. Free energy profiles for methoxide formation at 330 °C in H-SAPO-34 along the lowest free energy paths with barriers in kJ/mol. $(x{:}y)_{mw,sim}$ stands for a simulation with x MeOH and y H_2O molecules per BAS.

DOI: 10.1021/acscatal.5b02139
ACS Catal. 2016, 6, 1991−2002

additional protic molecules depends on the mixture composition. The free energy barriers reveal that methanol assists the methoxide formation reaction more efficiently than water. Indeed, for a $(1{:}0)_{mw,sim}$ loading, the reaction is not assisted, resulting in a relatively high free energy barrier of 167 ± 4 kJ/mol. For the high methanol loading $(5{:}0)_{mw,sim}$, the reaction always starts from a protonated methanol cluster (vide supra), which can adopt a favorable orientation for the methyl transfer with respect to the acid site prior to reaction. We reported earlier that these clusters mainly consist of two or three methanol molecules, which is also the case in this study.[53] As such, the reaction is always assisted as displayed in the snapshot shown in Figure 3b, resulting in a lowered free energy barrier (123 ± 2 kJ/mol). A similar effect was observed in H-ZSM-5 by some of the current authors.[62] For the $(1{:}4)_{mw,sim}$ methanol–water mixture, a less efficient methanol protonation was observed (vide supra). Furthermore, the loading of the pores is significantly lower when four methanol molecules are replaced by four water molecules. The lower density leads to fewer interactions between the protic molecules and thus a less efficient stabilization of the methoxide formation transition states. This is reflected in the fact that both paths in which the methoxide formation is assisted and unassisted by water molecules are sampled, as shown in the snapshots in Figure 3c. Consequently, a higher free energy barrier (147 ± 5 kJ/mol) for methoxide formation in the $(1{:}4)_{mw,sim}$ methanol–water mixture is found.

Summarizing, our set of metadynamics simulations suggests that the lower proton availability in the presence of water and the less efficient assisting role of water lower methanol's intrinsic reactivity toward methoxide formation, which is an elementary reaction step during methanol conversion and in particular during the induction period.

3.3. Implications of Methanol Reactivity on the Formation and Distribution of Carbocationic Reaction Intermediates at the Single-Particle Level. Our theoretical results suggest that water provokes a less efficient methanol and propene activation and lower methanol reactivity at the molecular level. To understand the implications of water at the single H-SAPO-34 crystal level, our simulations were combined with in situ UV–vis microspectroscopy experiments. Very interestingly, during the catalytic test we observed that the length of the induction period linearly increases with the water content of the feed as shown in Figure 5. The measurements were collected during the MTO reaction at 330 °C for a wide range of methanol–water mixtures with molar ratios of 1:0, 1:1, 1:2, 1:4, 1:8, and 1:12. The induction period was defined as the time until the first absorption band at 400 nm, corresponding to the active HP carbenium ions of methylated benzenes, appears in the UV–vis spectra. At this point, the formation of primary and secondary products starts as shown in Scheme 1. These results suggest that, next to methoxide, also aromatics formation is delayed with the addition of water, which is in line with our theoretical findings that methanol and propene are less efficiently activated and that the intrinsic methanol reactivity is decreased. These experiments confirm that the formation of the initial aromatic HP species is delayed by adding water to the feed.

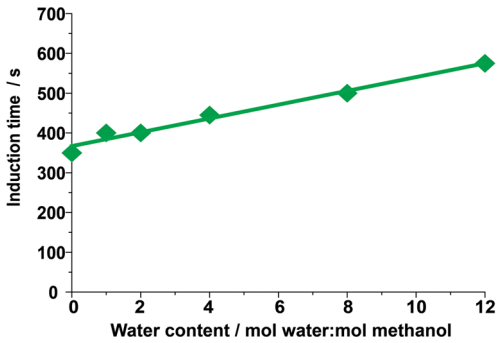

Figure 5. Induction time observed during the in situ UV–vis microspectroscopy measurements on single H-SAPO-34 crystals as a function of water content.

Simultaneously, optical micrographs were taken during the reaction and exhibited more homogeneous discoloration of the H-SAPO-34 crystals with increasing water content of the feed, as illustrated in Figure 6a–c. Prior to the MTO reaction, the H-SAPO-34 crystals are translucent. With a pure methanol feed, discoloration of the crystal to yellow-orange and brown-gray is very rapid and is mostly located in the rim of the crystal. When water is added, the crystals discolor more gradually from yellow to orange and finally to dark brown. Additionally, the spatial distribution of the discoloration is now more homogeneous throughout the crystal. More chemical information can be obtained by inspecting the time-resolved UV–vis spectra at the different methanol–water ratios. The spectra taken with a pure methanol feed show the evolution of a band at around 400 nm, which is ascribed to polymethylated benzene carbocations.[32] The evolution of other less pronounced bands at around 470 and 650 nm is due to the formation of larger aromatics, such as naphthalenic and phenanthrenic/pyrenic carbocations.[93] The addition of water to the reaction induces an increase in the total absorbance and considerable changes in the spectral features. More specifically, the absorbance at 400 nm increases and an even more pronounced increase was observed for the bands at higher wavelengths. This suggests that, upon water addition, more active and deactivating species are formed after the prolonged induction period and these are more homogeneously distributed in the H-SAPO-34 crystals due to a more efficient use of the catalyst crystals. Translating this back to Scheme 1 displaying the various stages of the MTO reaction, these experiments show that adding water increases the number of reaction intermediates for stages 3 and 4 of the MTO process.

The more homogeneous distribution and higher concentration of MTO intermediates upon cofeeding water were further demonstrated by in situ confocal fluorescence microscopy measurements. We used 488 and 561 nm excitation lines and fixed the sensitivity of the detectors to compare all the fluorescence images in a semiquantitative manner. The fluorescence microscopy images were acquired in a focal plane in the middle of the 50 × 50 × 50 μm H-SAPO-34 cubic crystals and the green and red fluorescent lights were superimposed, as illustrated in Figure 6d–f and also plotted as red-to-green fluorescence ratios in Figure S10 of the Supporting Information. The green and red fluorescent signals correspond to less and more extended aromatic coke species, respectively.[33] At first glance, when water is present, the overall intensity of the fluorescence is higher, indicating a higher concentration of fluorescent aromatics inside the single H-SAPO-34 crystals.

Additionally, the results show that the fluorescence is mostly located at the periphery of the H-SAPO-34 crystal, in an eggshell-type distribution, when water is not present. This is in sharp contrast to the fluorescence when water is added to the

DOI: 10.1021/acscatal.5b02139
ACS Catal. 2016, 6, 1991–2002

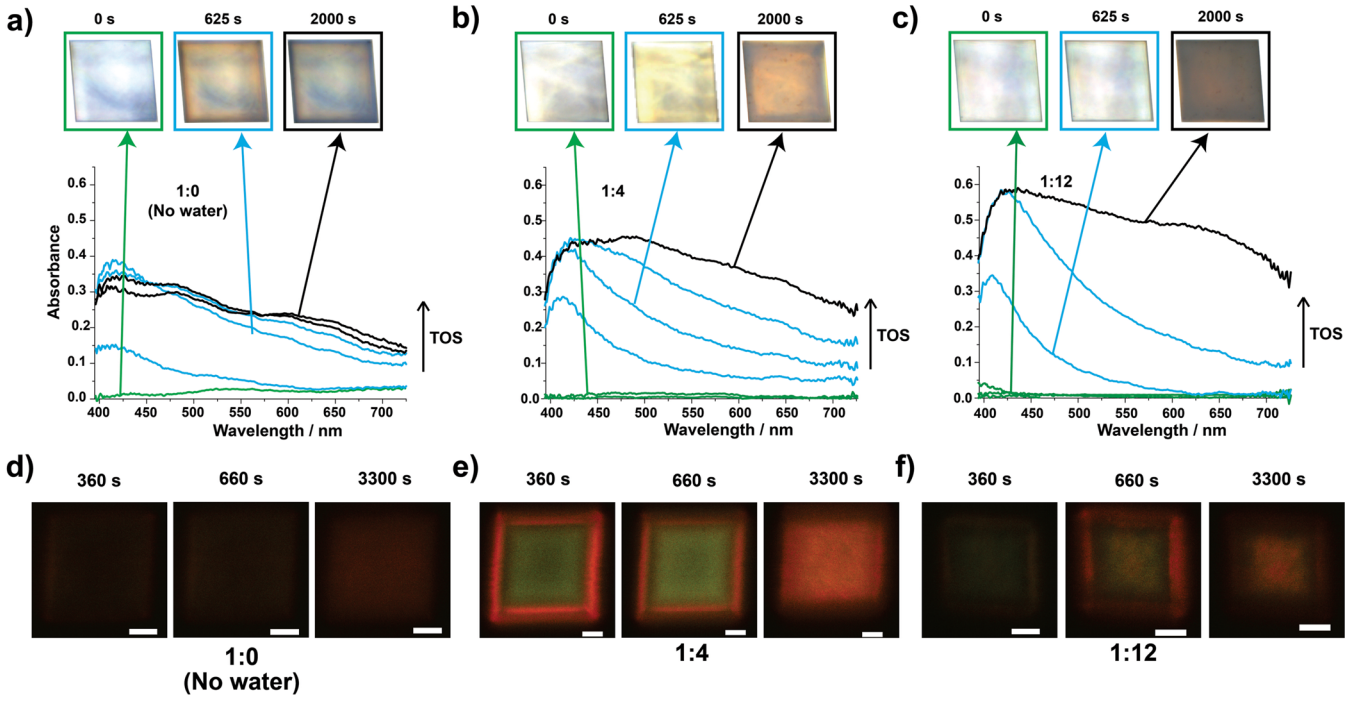

Figure 6. (a–c) Optical images and UV–vis spectra of single H-SAPO-34 crystals with time on stream during the methanol-to-olefins (MTO) reaction with different methanol–water ratios of (a) 1:0, (b) 1:4, and (c) 1:12. The colors of the UV–vis spectra indicate the evolution of the reaction from the induction period (green) to the formation of aromatics (blue) and the deactivation (black) of the single crystals. (d–f) Confocal fluorescence microscopy images of single H-SAPO-34 crystals during the MTO reaction with different methanol–water ratios of (d) 1:0, (e) 1:4, and (f) 1:12. The images were taken in the middle plane of the crystal. The colors in the fluorescent images originate from the overlap of two profiles with a laser excitation of λ = 488 nm (detection at λ = 500–550 nm) and λ = 561 nm (detection at λ = 570–620 nm).

reaction, where a more homogeneous distribution is observed in agreement with the optical micrographs in Figure 6a–c. The distribution of the two different fluorescence signals also depends on the presence and concentration of water in the feed. To be more specific, without water the fluorescent signal is mostly red, which is an indication that large aromatic species are formed, in the outer layer, while the signal is more yellow (i.e., indicative of small and large species being formed simultaneously) toward the inside of the crystal. When water is added to the reaction feed, the outer layer is also red, but the inner part is mostly green, turning gradually into yellow. This indicates that the addition of water preserves small aromatics inside the crystal for a longer period and these species are eventually converted into larger aromatics with increasing time on stream. Additionally, during these experiments we observed the formation of a layer mainly consisting of large non-fluorescent coke-like species. This layer is located at the rim of the H-SAPO-34 crystals and first showed very intense red fluorescence and then very little fluorescence.[93−95] The measured thickness of this coke layer is displayed in Figure 7 and shows a linear increase with the amount of water in the reaction. The thicker coke crust after water addition shows that the catalyst material is still accessible for methanol when some initial coke molecules have been formed. This again points toward the more efficient utilization of the catalyst crystals.

The cofeeding of water during the reaction might cause the formation of mesoporosity in the H-SAPO-34 crystals. These changes in the textural properties of the material could account for the more homogeneous formation of coke species throughout the individual crystals. To evaluate whether the reaction conditions could indeed induce mesopore formation, we performed a control experiment by steaming H-SAPO-34 at

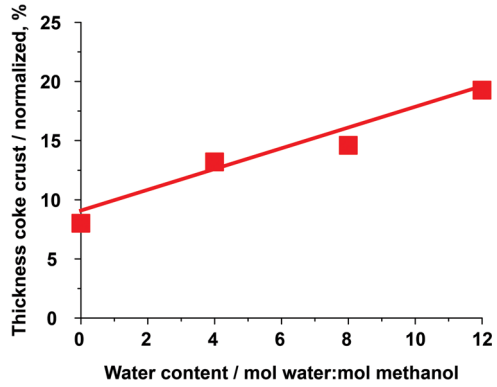

Figure 7. Thickness of the coke crust (normalized to the crystal size) observed during the confocal fluorescence microscopy measurements as a function of water content. The thickness was calculated from the confocal fluorescence images by subtracting the size of the crystal not displaying red fluorescence from the total size of the crystal.

a temperature even higher than the reaction temperature (350 °C). After steaming, we added Nile Blue A to the H-SAPO-34 crystals, which enables mesopore visualization with confocal fluorescence microscopy as previously described.[96] The fluorescence microscopy image of the steamed H-SAPO-34 sample in Figure S11b in the Supporting Information shows that fluorescence is in the noise level and therefore no fluorescent dye has been adsorbed on the single crystals. This validates that steaming under the applied reaction conditions created no (noticeable amounts of) mesopores.

Our experimental results on single catalyst crystals show that water significantly increases the length of the induction period, which can be correlated with less efficient methanol and

DOI: 10.1021/acscatal.5b02139
ACS Catal. 2016, 6, 1991−2002

Scheme 5. Schematic of the Effect of Water Addition on the Methanol-to-Olefin (MTO) Reaction and the Related Formation of Different Aromatic and Polyaromatic Species

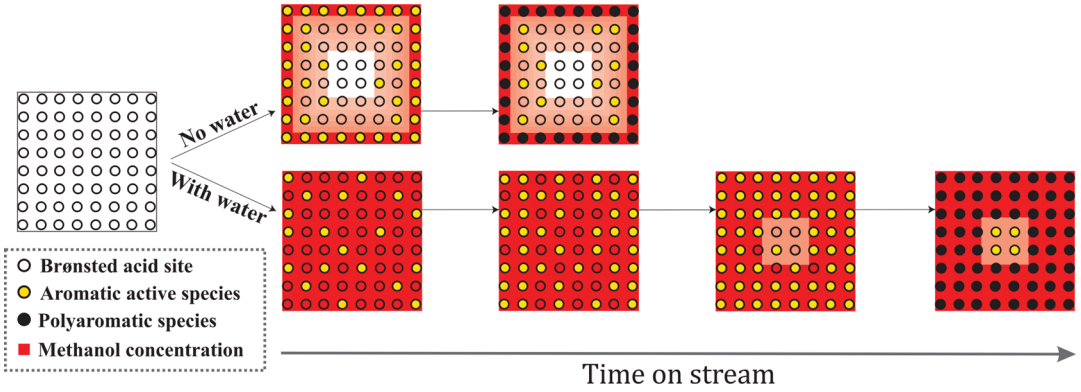

propene activation and lower intrinsic methanol reactivity found in the molecular dynamics and metadynamics simulations. Our simulations in particular suggest that water occupying a BAS prevents catalysis of reactive events. In particular, water prevents propene from forming bulky cyclic hydrocarbons that remain trapped in the cages of the small-pore H-SAPO-34 material. Water thus enables a better distribution of MTO reaction intermediates due to a better accessibility of the inner parts of the catalyst crystals for small molecules such as methanol and propene. This eventually leads to a more efficient use of the catalyst crystals.

4. CONCLUSIONS

We have evaluated the effect of water on the methanol-to-olefins reaction in the archetypal H-SAPO-34 material by a combined theoretical and experimental approach. A thorough understanding of the impact of water on the various stages of the MTO conversion is needed, given that the addition of appropriate amounts of water to the feed may lead to optimized product selectivity and catalyst stability.[9,10,12] Many of these observations in earlier studies have been related to water occupying an important fraction of the acid sites. To obtain deeper insight into this hypothesis at the molecular and microscopic level, a complementary theoretical and experimental approach was followed to investigate the impact of water on various stages of the MTO process. A summary of our findings is sketched in Scheme 5. Our results at the molecular level indeed confirm the suggested hypothesis of competitive adsorption between methanol and water. As a result, lower proton availability for methanol and thus less efficient methanol protonation were observed. A similar competitive effect was also observed for water and propene, suggesting that dimerization and cyclization might be hampered by water. As such, water can moderate the formation of bulky HP species that cannot diffuse through the small-pore material. The occupation of the acid sites by water ultimately leads to reduced pore blocking, enhancing the diffusion of methanol and small olefins deeper into the crystals to undergo reactive events. Apart from this, the intrinsic methanol reactivity, traced by studying formation of framework-bound methoxide species, was found to be lower in a methanol–water mixture. This could be attributed to the fact that additional protic molecules facilitate the reaction, but this assisting effect is less efficient with water than with methanol. Since methoxides are predominant species during the early stages of the MTO reaction—i.e. the equilibration and induction period as indicated in Scheme 1—the retarding effect of water addition on the kinetics of methoxide formation increases the length of the induction period, as seen in the UV–vis experiments on a single-particle level. Furthermore, methoxides are also reactive methylating agents that can play a role during the formation of primary and secondary products. Decreased intrinsic methanol reactivity and reduced accessibility for olefins such as propene to the BAS might thus result in the slower formation of HP species, which alleviates molecular diffusion limitations and therefore enables methanol and propene to diffuse deeper into the catalyst crystals. That methanol and other small reactive molecules have better access to the inner part of the crystals is reflected in a more homogeneous distribution of MTO intermediates and deactivating coke species, as shown by our UV–vis microspectroscopy and in situ confocal fluorescence experiments. Water thus induces a more efficient use of the catalyst crystals. Going back to Scheme 1, we confirm that adding water to the methanol feed affects all four reaction stages of the MTO process.

The results are in agreement with earlier reported enhanced catalyst stability and higher conversions of methanol in the presence of water.[9,11,19,39,40] Our combined theory–experiment approach has a high potential for the study of other zeolite-catalyzed processes in which competition between guest molecules might influence the type and spatial distribution of reaction intermediates and deactivation products. It should be noted that the effect of water on MTO might be substantially different in other zeolite or zeotype materials. Further studies on the intricate impact of water on the entire catalytic cycles and product selectivity are mandatory. Hereby, creatively designed theoretical and experimental methodologies will again go hand in hand.

■ ASSOCIATED CONTENT

Supporting Information

The Supporting Information is available free of charge on the ACS Publications website at DOI: 10.1021/acscatal.5b02139.

Additional computational and experimental details, more information on the methanol and water adsorption simulations, calculated velocity power spectra, additional confocal fluorescence microscopy images, and results on catalyst steaming (PDF)

DOI: 10.1021/acscatal.5b02139
ACS Catal. 2016, 6, 1991–2002

AUTHOR INFORMATION

Corresponding Authors

*E-mail for E.J.M.: e.j.meijer@uva.nl.
*E-mail for B.M.W.: B.M.Weckhuysen@uu.nl.
*E-mail for V.V.S.: veronique.vanspeybroeck@ugent.be.
*E-mail for J.R.-M.: J.RuizMartinez@uu.nl.

Notes

The authors declare no competing financial interest.

ACKNOWLEDGMENTS

K.D.W., K.H. and V.V.S. thank the Foundation of Scientific Research-Flanders (FWO), the Research Board of Ghent University, BELSPO (IAP P7/05), and the European Union's Horizon 2020 research and innovation programm (consolidator ERC grant agreement No. 647755-DYNPOR (2015−2020)). Computational resources and services were provided by the Stevin Supercomputer Infrastructure of Ghent University and by the Flemish Supercomputer Center (VSC), funded by the Hercules Foundation and the Flemish Government-department EWI. This work is part of the research program of the "Stichting voor Fundamenteel Onderzoek der Materie" (FOM), which is financially supported by the 'Nederlandse Organisatie voor Wetenschappelijk Onderzoek' (NWO). J.R.-M. also acknowledges CW-NWO for his VENI personal grant.

REFERENCES

(1) Chen, K.; Damron, J.; Pearson, C.; Resasco, D.; Zhang, L.; White, J. L. *ACS Catal.* **2014**, *4*, 3039−3044.
(2) Jacobs, P. A.; Dusselier, M.; Sels, B. F. *Angew. Chem., Int. Ed.* **2014**, *53*, 8621−8626.
(3) Olsbye, U.; Svelle, S.; Lillerud, K. P.; Wei, Z. H.; Chen, Y. Y.; Li, J. F.; Wang, J. G.; Fan, W. B. *Chem. Soc. Rev.* **2015**, *44*, 7155−7176.
(4) Stöcker, M. *Microporous Mesoporous Mater.* **1999**, *29*, 3−48.
(5) Olsbye, U.; Svelle, S.; Bjørgen, M.; Beato, P.; Janssens, T. V. W.; Joensen, F.; Bordiga, S.; Lillerud, K. P. *Angew. Chem., Int. Ed.* **2012**, *51*, 5810−5831.
(6) Hemelsoet, K.; Van der Mynsbrugge, J.; De Wispelaere, K.; Waroquier, M.; Van Speybroeck, V. *ChemPhysChem* **2013**, *14*, 1526−1545.
(7) Lefevere, J.; Mullens, S.; Meynen, V.; Van Noyen, J. *Chem. Pap.* **2014**, *68*, 1143−1153.
(8) Keil, F. J. *Microporous Mesoporous Mater.* **1999**, *29*, 49−66.
(9) Marchi, A. J.; Froment, G. F. *Appl. Catal.* **1991**, *71*, 139−152.
(10) Wu, X.; Anthony, R. G. *Appl. Catal., A* **2001**, *218*, 241−250.
(11) Marchi, A. J.; Froment, G. F. *Appl. Catal., A* **1993**, *94*, 91−106.
(12) Kumita, Y.; Gascon, J.; Stavitski, E.; Moulijn, J. A.; Kapteijn, F. *Appl. Catal., A* **2011**, *391*, 234−243.
(13) Park, Y. K.; Baek, S. W.; Ihm, S. K. *J. Ind. Eng. Chem.* **2001**, *7*, 167−172.
(14) Ilias, S.; Bhan, A. *ACS Catal.* **2013**, *3*, 18−31.
(15) Lesthaeghe, D.; Van Speybroeck, V.; Marin, G. B.; Waroquier, M. *Ind. Eng. Chem. Res.* **2007**, *46*, 8832−8838.
(16) Khadzhiev, S. N.; Magomedova, M. V.; Peresypkina, E. G. *Pet. Chem.* **2014**, *54*, 245−269.
(17) Lesthaeghe, D.; Van Speybroeck, V.; Marin, G. B.; Waroquier, M. *Angew. Chem., Int. Ed.* **2006**, *45*, 1714−1719.
(18) Van Speybroeck, V.; De Wispelaere, K.; Van der Mynsbrugge, J.; Vandichel, M.; Hemelsoet, K.; Waroquier, M. *Chem. Soc. Rev.* **2014**, *43*, 7326−7357.
(19) Wang, W.; Buchholz, A.; Seiler, M.; Hunger, M. *J. Am. Chem. Soc.* **2003**, *125*, 15260−15267.
(20) Dahl, I. M.; Kolboe, S. *J. Catal.* **1996**, *161*, 304−309.
(21) Dahl, I. M.; Kolboe, S. *J. Catal.* **1994**, *149*, 458−464.
(22) Dahl, I. M.; Kolboe, S. *Catal. Lett.* **1993**, *20*, 329−336.
(23) Song, W. G.; Fu, H.; Haw, J. F. *J. Am. Chem. Soc.* **2001**, *123*, 4749−4754.
(24) Hereijgers, B. P. C.; Bleken, F.; Nilsen, M. H.; Svelle, S.; Lillerud, K. P.; Bjørgen, M.; Weckhuysen, B. M.; Olsbye, U. *J. Catal.* **2009**, *264*, 77−87.
(25) Vandichel, M.; Lesthaeghe, D.; Van der Mynsbrugge, J.; Waroquier, M.; Van Speybroeck, V. *J. Catal.* **2010**, *271*, 67−78.
(26) Li, J. F.; Wei, Z. H.; Chen, Y. Y.; Jing, B. Q.; He, Y.; Dong, M.; Jiao, H. J.; Li, X. K.; Qin, Z. F.; Wang, J. G.; Fan, W. B. *J. Catal.* **2014**, *317*, 277−283.
(27) Dai, W.; Wang, C.; Dyballa, M.; Wu, G.; Guan, N.; Li, L.; Xie, Z.; Hunger, M. *ACS Catal.* **2015**, *5*, 317−326.
(28) Song, W. G.; Haw, J. F.; Nicholas, J. B.; Heneghan, C. S. *J. Am. Chem. Soc.* **2000**, *122*, 10726−10727.
(29) Qian, Q.; Vogt, C.; Mokhtar, M.; Asiri, A. M.; Al-Thabaiti, S. A.; Basahel, S. N.; Ruiz-Martínez, J.; Weckhuysen, B. M. *ChemCatChem* **2014**, *6*, 3396−3408.
(30) Wang, C. M.; Wang, Y. D.; Xie, Z. K.; Liu, Z. P. *J. Phys. Chem. C* **2009**, *113*, 4584−4591.
(31) De Wispelaere, K.; Hemelsoet, K.; Waroquier, M.; Van Speybroeck, V. *J. Catal.* **2013**, *305*, 76−80.
(32) Hemelsoet, K.; Qian, Q.; De Meyer, T.; De Wispelaere, K.; De Sterck, B.; Weckhuysen, B. M.; Waroquier, M.; Van Speybroeck, V. *Chem. - Eur. J.* **2013**, *19*, 16595−16606.
(33) Qian, Q.; Ruiz-Martínez, J.; Mokhtar, M.; Asiri, A. M.; Al-Thabaiti, S. A.; Basahel, S. N.; van der Bij, H. E.; Kornatowski, J.; Weckhuysen, B. M. *Chem. - Eur. J.* **2013**, *19*, 11204−11215.
(34) Van Speybroeck, V.; Hemelsoet, K.; De Wispelaere, K.; Qian, Q.; Van der Mynsbrugge, J.; De Sterck, B.; Weckhuysen, B. M.; Waroquier, M. *ChemCatChem* **2013**, *5*, 173−184.
(35) Borodina, E.; Meirer, F.; Lezcano-González, I.; Mokhtar, M.; Asiri, A. M.; Al-Thabaiti, S. A.; Basahel, S. N.; Ruiz-Martínez, J.; Weckhuysen, B. M. *ACS Catal.* **2015**, *5*, 992−1003.
(36) Chen, D.; Moljord, K.; Holmen, A. *Microporous Mesoporous Mater.* **2012**, *164*, 239−250.
(37) Müller, S.; Liu, Y.; Vishnuvarthan, M.; Sun, X.; van Veen, A. C.; Haller, G. L.; Sanchez-Sanchez, M.; Lercher, J. A. *J. Catal.* **2015**, *325*, 48−59.
(38) Haw, J. F.; Marcus, D. M. *Top. Catal.* **2005**, *34*, 41−48.
(39) Chen, J. Q.; Bozzano, A.; Glover, B.; Fuglerud, T.; Kvisle, S. *Catal. Today* **2005**, *106*, 103−107.
(40) Chang, C. D.; Lang, W. H.; Silvestri, A. J. Mobil Oil Corporation, U.S. Patent US4062905 A, 1977.
(41) Yang, M.; Tian, P.; Wang, C.; Yuan, Y.; Yang, Y.; Xu, S.; He, Y.; Liu, Z. *Chem. Commun.* **2014**, *50*, 1845−1847.
(42) Álvaro-Munoz, T.; Marquez-Alvarez, C.; Sastre, E. *Catal. Today* **2012**, *179*, 27−34.
(43) Álvaro-Muñoz, T.; Márquez-Álvarez, C.; Sastre, E. *Appl. Catal., A* **2014**, *472*, 72−79.
(44) Wu, L.; Hensen, E. J. M. *Catal. Today* **2014**, *235*, 160−168.
(45) Shahda, M.; Dengchao, Y.; Huixin, W. *Pet. Sci. Technol.* **2008**, *26*, 1893−1903.
(46) Taheri Najafabadi, A.; Fatemi, S.; Sohrabi, M.; Salmasi, M. *J. Ind. Eng. Chem.* **2012**, *18*, 29−37.
(47) Caesar, P. D.; Morrison, R. A. Mobil Oil Corporation (New York, NY), U.S. Patent US4083889, 1978.
(48) Seddon, D.; Mole, T.; Whiteside, J. A. Imperial Chemical Industries PLC (London), U.S. Patent US4499314, 1985.
(49) Kaiser, S. W. Union Carbide Corporation (Danbury, CT), U.S. Patent US4524234, 1985.
(50) Tjandra, S.; Anthony, R. G.; Akgerman, A. *Ind. Eng. Chem. Res.* **1993**, *32*, 2602−2607.
(51) Yin, X.; Leung, D. Y. C.; Chang, J.; Wang, J.; Fu, Y.; Wu, C. *Energy Fuels* **2005**, *19*, 305−310.
(52) Demirbas, A. *Prog. Energy Combust. Sci.* **2007**, *33*, 1.
(53) De Wispelaere, K.; Ensing, B.; Ghysels, A.; Meijer, E. J.; Van Speybroeck, V. *Chem. - Eur. J.* **2015**, *21*, 9385−9396.
(54) Benco, L.; Bučko, T.; Hafner, J. *J. Catal.* **2011**, *277*, 104−116.
(55) Bučko, T.; Benco, L.; Hafner, J.; Angyan, J. G. *J. Catal.* **2011**, *279*, 220−228.
(56) Bučko, T.; Hafner, J. *J. Catal.* **2015**, *329*, 32−48.

DOI: 10.1021/acscatal.5b02139
ACS Catal. 2016, 6, 1991−2002

(57) Göltl, F.; Hafner, J. *Microporous Mesoporous Mater.* **2013**, *166*, 176−184.
(58) Jiang, T.; Göltl, F.; Bulo, R. E.; Sautet, P. *ACS Catal.* **2014**, *4*, 2351−2358.
(59) Gomes, J.; Head-Gordon, M.; Bell, A. T. *J. Phys. Chem. C* **2014**, *118*, 21409−21419.
(60) Zimmerman, P. M.; Tranca, D. C.; Gomes, J.; Lambrecht, D. S.; Head-Gordon, M.; Bell, A. T. *J. Am. Chem. Soc.* **2012**, *134*, 19468−19476.
(61) Moors, S. L. C.; De Wispelaere, K.; Van der Mynsbrugge, J.; Waroquier, M.; Van Speybroeck, V. *ACS Catal.* **2013**, *3*, 2556−2567.
(62) Van der Mynsbrugge, J.; Moors, S. L. C.; De Wispelaere, K.; Van Speybroeck, V. *ChemCatChem* **2014**, *6*, 1906−1918.
(63) Hutter, J.; Iannuzzi, M.; Schiffmann, F.; VandeVondele, J. *Wiley Interdiscip. Rev.: Comput. Mol. Sci.* **2014**, *4*, 15.
(64) Grimme, S.; Antony, J.; Ehrlich, S.; Krieg, H. *J. Chem. Phys.* **2010**, *132*, 154104.
(65) Vanduyfhuys, L.; Ghysels, A.; Rogge, S. M. J.; Demuynck, R.; Van Speybroeck, V. *Mol. Simul.* **2015**, *41*, 1311−1328.
(66) Chiu, C. C.; Vayssilov, G. N.; Genest, A.; Borgna, A.; Rosch, N. *J. Comput. Chem.* **2014**, *35*, 809−819.
(67) First, E. L.; Gounaris, C. E.; Wei, J.; Floudas, C. A. *Phys. Chem. Chem. Phys.* **2011**, *13*, 17339−17358.
(68) Kuhn, J.; Castillo-Sanchez, J. M.; Gascon, J.; Calero, S.; Dubbeldam, D.; Vlugt, T. J. H.; Kapteijn, F.; Gross, J. *J. Phys. Chem. C* **2009**, *113*, 14290−14301.
(69) Barducci, A.; Bonomi, M.; Parrinello, M. *Wiley Interdiscip. Rev.: Comput. Mol. Sci.* **2011**, *1*, 826.
(70) Ensing, B.; De Vivo, M.; Liu, Z. W.; Moore, P.; Klein, M. L. *Acc. Chem. Res.* **2006**, *39*, 73−81.
(71) Laio, A.; Gervasio, F. L. *Rep. Prog. Phys.* **2008**, *71*, 126601.
(72) Sutto, L.; Marsili, S.; Gervasio, F. L. *Wiley Interdiscip. Rev.: Comput. Mol. Sci.* **2012**, *2*, 771.
(73) Ensing, B.; Laio, A.; Parrinello, M.; Klein, M. L. *J. Phys. Chem. B* **2005**, *109*, 6676−6687.
(74) Karwacki, L.; Stavitski, E.; Kox, M. H. F.; Kornatowski, J.; Weckhuysen, B. M. *Angew. Chem., Int. Ed.* **2007**, *46*, 7228−7231.
(75) Van der Mynsbrugge, J.; Hemelsoet, K.; Vandichel, M.; Waroquier, M.; Van Speybroeck, V. *J. Phys. Chem. C* **2012**, *116*, 5499−5508.
(76) Lee, C. C.; Gorte, R. J.; Farneth, W. E. *J. Phys. Chem. B* **1997**, *101*, 3811−3817.
(77) Olson, D. H.; Haag, W. O.; Borghard, W. S. *Microporous Mesoporous Mater.* **2000**, *35*−*36*, 435−446.
(78) Hotevar, S.; Levec, J. *J. Catal.* **1992**, *135*, 518−532.
(79) Hemelsoet, K.; Nollet, A.; Van Speybroeck, V.; Waroquier, M. *Chem. - Eur. J.* **2011**, *17*, 9083−9093.
(80) Lo, C.; Giurumescu, C. A.; Radhakrishnan, R.; Trout, B. L. *Mol. Phys.* **2004**, *102*, 281−288.
(81) Sauer, J.; Sierka, M.; Haase, F. In *Transitions State Modeling for Catalysis*; Morokuma, K., Truhlar, D. G., Eds.; American Chemical Society: Washington DC, 1999; Vol. *721*, pp 358−367.
(82) Haase, F.; Sauer, J.; Hutter, J. *Chem. Phys. Lett.* **1997**, *266*, 397.
(83) Stich, I.; Gale, J. D.; Terakura, K.; Payne, M. C. *J. Am. Chem. Soc.* **1999**, *121*, 3292−3302.
(84) Gale, J. D.; Shah, R.; Payne, M. C.; Stich, I.; Terakura, K. *Catal. Today* **1999**, *50*, 525−532.
(85) Termath, V.; Haase, F.; Sauer, J.; Hutter, J.; Parrinello, M. *J. Am. Chem. Soc.* **1998**, *120*, 8512−8516.
(86) Jeanvoine, Y.; Angyan, J. G.; Kresse, G.; Hafner, J. *J. Phys. Chem. B* **1998**, *102*, 5573−5580.
(87) Vener, M. V.; Rozanska, X.; Sauer, J. *Phys. Chem. Chem. Phys.* **2009**, *11*, 1702−1712.
(88) Joshi, K. L.; Psofogiannakis, G.; van Duin, A. C. T.; Raman, S. *Phys. Chem. Chem. Phys.* **2014**, *16*, 18433−18441.
(89) Qi, L.; Wei, Y. X.; Xu, L.; Liu, Z. M. *ACS Catal.* **2015**, *5*, 3973−3982.
(90) Brogaard, R. Y.; Henry, R.; Schuurman, Y.; Medford, A. J.; Moses, P. G.; Beato, P.; Svelle, S.; Nørskov, J. K.; Olsbye, U. *J. Catal.* **2014**, *314*, 159−169.
(91) Jiang, Y. J.; Hunger, M.; Wang, W. *J. Am. Chem. Soc.* **2006**, *128*, 11679−11692.
(92) Wang, W.; Hunger, M. *Acc. Chem. Res.* **2008**, *41*, 895−904.
(93) Mores, D.; Kornatowski, J.; Olsbye, U.; Weckhuysen, B. M. *Chem. - Eur. J.* **2011**, *17*, 2874−2884.
(94) Hofmann, J. P.; Mores, D.; Aramburo, L. R.; Teketel, S.; Rohnke, M.; Janek, J.; Olsbye, U.; Weckhuysen, B. M. *Chem. - Eur. J.* **2013**, *19*, 8533−8542.
(95) Mores, D.; Stavitski, E.; Kox, M. H. F.; Kornatowski, J.; Olsbye, U.; Weckhuysen, B. M. *Chem. - Eur. J.* **2008**, *14*, 11320−11327.
(96) Buurmans, I. L. C.; Ruiz-Martínez, J.; Knowles, W. V.; van der Beek, D.; Bergwerff, J. A.; Vogt, E. T. C.; Weckhuysen, B. M. *Nat. Chem.* **2011**, *3*, 862.

DOI: 10.1021/acscatal.5b02139
ACS Catal. 2016, 6, 1991−2002